Analytical and Bioanalytical Chemistry
https://doi.org/10.1007/s00216-020-02391-4

RESEARCH PAPER

Metabolite profiling of human blood by surface-enhanced Raman spectroscopy for surgery assessment and tumor screening in breast cancer

Duo Lin[1] · Yunyi Wang[2] · Tingyin Wang[2] · Youzhi Zhu[3] · Xueliang Lin[2] · Yao Lin[4] · Shangyuan Feng[2]

Received: 5 October 2019 / Revised: 26 December 2019 / Accepted: 6 January 2020

Abstract

Mammography, a standard screening method for breast cancer, is effective for reducing the rate of death; however, it suffers from frequent false positive alarm and radiation risk. Besides, surgery treatment has a vital impact on the clinical outcomes of breast cancer, offering enormous benefits for breast cancer care and management. In this work, we analyzed the peripheral blood sample from breast cancer patients with pre- and post-surgery and healthy volunteers using label-free surface-enhanced Raman spectroscopy technology based on silver nanoparticles. Results showed that distinct patterns of blood belonging to specific subjects could be profiled, and corresponding accuracies of 95% and 100% were achieved by multivariate diagnostic algorithm for pre-surgery vs. post-surgery and pre-surgery vs. normal groups, respectively, providing a unique blood analysis method for surgery evaluation as well as tumor screening in breast cancer.

Keywords Surface-enhanced Raman spectroscopy · Silver nanoparticles · Blood analysis · Breast cancer · Surgery assessment · Screening

Introduction

With an estimated 2 billion new cases in 2018, breast cancer has become the most commonly diagnosed cancer and the leading cause of mortality among women worldwide, posing a tremendous threat on female heathy [1]. Effective and early screening followed by surgery and chemotherapy/radiotherapy procedure will contribute to a significant decline in mortality. Currently, the most commonly used screening method is mammography examination [2]. While highly effective for reducing the rate of death from breast cancer, mammography still suffers from some limitations, such as low sensitivity in breast tissue with greater density, frequent false positive alarm, and radiation risk [3, 4]. Technological advances in gene sequencing of tumor-related circulating DNA have offer a unique and promising approach for breast cancer detection; however, some challenges including high-cost, complex procedure and uncertain clinical utility need to be urgently addressed [5, 6]. Therefore, development of a non-invasive, rapid, convenient, and sensitive method for breast cancer detection is highly required in clinical practice.

Electronic supplementary material The online version of this article (https://doi.org/10.1007/s00216-020-02391-4) contains supplementary material, which is available to authorized users.

✉ Youzhi Zhu
zhu@fjmu.edu.cn

✉ Yao Lin
yaolin@fjnu.edu.cn

✉ Shangyuan Feng
syfeng@fjnu.edu.cn

[1] College of Integrated Traditional Chinese and Western Medicine, Fujian University of Traditional Chinese Medicine, Fuzhou 350122, Fujian, China

[2] Key Laboratory of OptoElectronic Science and Technology for Medicine, Ministry of Education, Digital Fujian Internet-of-Things Laboratory of Environment Monitoring, Fujian Provincial Key Laboratory for Photonics Technology, Fujian Normal University, Fuzhou 350007, Fujian, China

[3] Department of Thyroid and Breast Surgery, First Affiliated Hospital of Fujian Medical University, Fuzhou 350001, Fujian, China

[4] College of Life Sciences, Fujian Normal University, Fuzhou 350007, Fujian, China

Published online: 21 January 2020

Surface-enhanced Raman spectroscopy (SERS) technology based on optical inelastic scattering has recently emerged as one of the most powerful analytical methods. Owing to the coupling of incident electromagnetic field in the gap between nanoscale metallic materials (gold or silver nanoparticles), the bio-targets adsorbed or highly close to these roughened metallic surfaces will generate a dramatically enhanced Raman signals, allowing us to explore rich structural and quantitative information, even at single molecular lever in some cases [7]. Increasing evidences have shown that SERS holds a great promise for biomedical applications, ranging from DNA [8, 9] and cell [10, 11] to blood [12, 13] and tissue [14] samples. Amount them, novel studies on blood analysis using SERS for breast cancer detection have attracted much attention. For instance, Sha's group used a combination of magnetic particles and nanoplex biotags to capture and detect breast cancer cells in whole blood using label-based SERS technology, which was promising for circulating tumor cell's detection [15]. Cui's group developed a microfluidic chip–based SERS to simultaneously detect multiple breast cancer biomarkers in blood sample, providing a novel immunoassay biosensor for breast cancer detection [16]. Besides, the sensitive SERS technology was applied by Bonifacio [17] and González-Solís [18] groups for direct blood analysis with the aim of breast cancer diagnosis. While exciting advances in breast cancer diagnosis using blood SERS, few studies focus on the surgery treatment effect via blood analysis using SERS. As we all known, surgery is essential and offers enormous benefits for cancer care and management, due to its ability of being preventive, diagnostic, curative, supportive, palliative, and reconstructive. For advanced breast cancers, mastectomy is crucial for palliative care. Additionally, the interval between diagnosis and surgery proves to greatly affect the survival outcomes in early breast cancer [19, 20].

In the context of that, we profile the blood samples from breast cancer patients with pre- and post-surgery using label-free SERS technology in this work, with the aim to evaluate the surgery treatment effect for breast cancer. Besides, we further analyze the contribution of hypoxanthine and uric acid to the discriminant results achieved by this blood SERS method for breast cancer detection.

Materials and methods

Blood sample collection

This assay involved 30 blood serum samples from breast cancer patients before surgery and 30 blood serum samples from the same patients after surgery. The mean age of patients is 54.9, and the median age is 56. Additionally, 10 of them belong to starting cancer state and the rest of them are advanced state with metastasis. More details are represented in Table S1 (see Electronic Supplementary Material, ESM). Besides, a total of 30 blood serum samples from non-cancer volunteers was included here as the control (Fig. 1a). All these samples were collected from the First Affiliated Hospital of Fujian Medical University. This assay was approved by the ethics committee and every patient signed an informed consent before blood collection. Prior to SERS measurement, serum samples were stored in a freezer at − 80 °C.

Silver nanoparticles' preparation and characteristics

Silver nanoparticles (Ag NPs) were prepared through reducing hydroxylamine according to the method proposed by Leopold [21]. Figure 1b shows the diameter of prepared Ag NPs is approximately 45 nm shown by TEM image. The corresponding maximum absorption peak is located at 418 nm. Zeta potential measurement demonstrates that the surface potential of Ag NPS is − 15.5 mV shown in Fig. 1c. And the SERS enhancement factor of prepared Ag colloids is approximately 4×10^6. Besides, the x-ray diffraction (XRD) pattern recorded from Ag NPs is displayed in Fig. 1d, and four peaks at 2θ values of 38.1°, 44.2°, 64.4°, and 77.4° can be observed, corresponding to (111), (200), (220), and (311) planes for silver, respectively [22]. Before use, the prepared Ag NP should be concentrated by centrifugation at 10,000 r/min for 10 min.

Blood SERS measurement

Same volume of each serum sample (5 μL) and Ag NPs (5 μL) were mixed uniformly on an aluminum plate for 2 h at room temperature. Then, the SERS spectrum of blood Ag NPs' mixture was measured in the range of 400–1800 cm^{-1} using a confocal Raman micro-spectrometer (Renishaw, Great Britain). The near-infrared laser source (785 nm) was used to excite the samples via × 20 objective with 10-s acquisition time. For each blood sample, three spectra were collected from random locations, and the mean spectrum was calculated to represent this sample. Prior to Raman measurement, a silica plate with the standard Raman signal at 520 cm^{-1} was used to calibrate the system.

Data analysis

A multi-polynomial fitting algorithm was firstly used to remove the fluorescence background of each raw SERS spectrum. Then, all SERS spectra were normalized to minimize the influences caused by the fluctuation of laser power, enabling a better comparison of the spectral shapes and relative peak intensities. A workflow of the spectral data preprocessing was represented in Fig. S1 (see ESM). Besides, principle component analysis combined with linear discriminant analysis (PCA-LDA) [23–26] was used to differentiate different blood

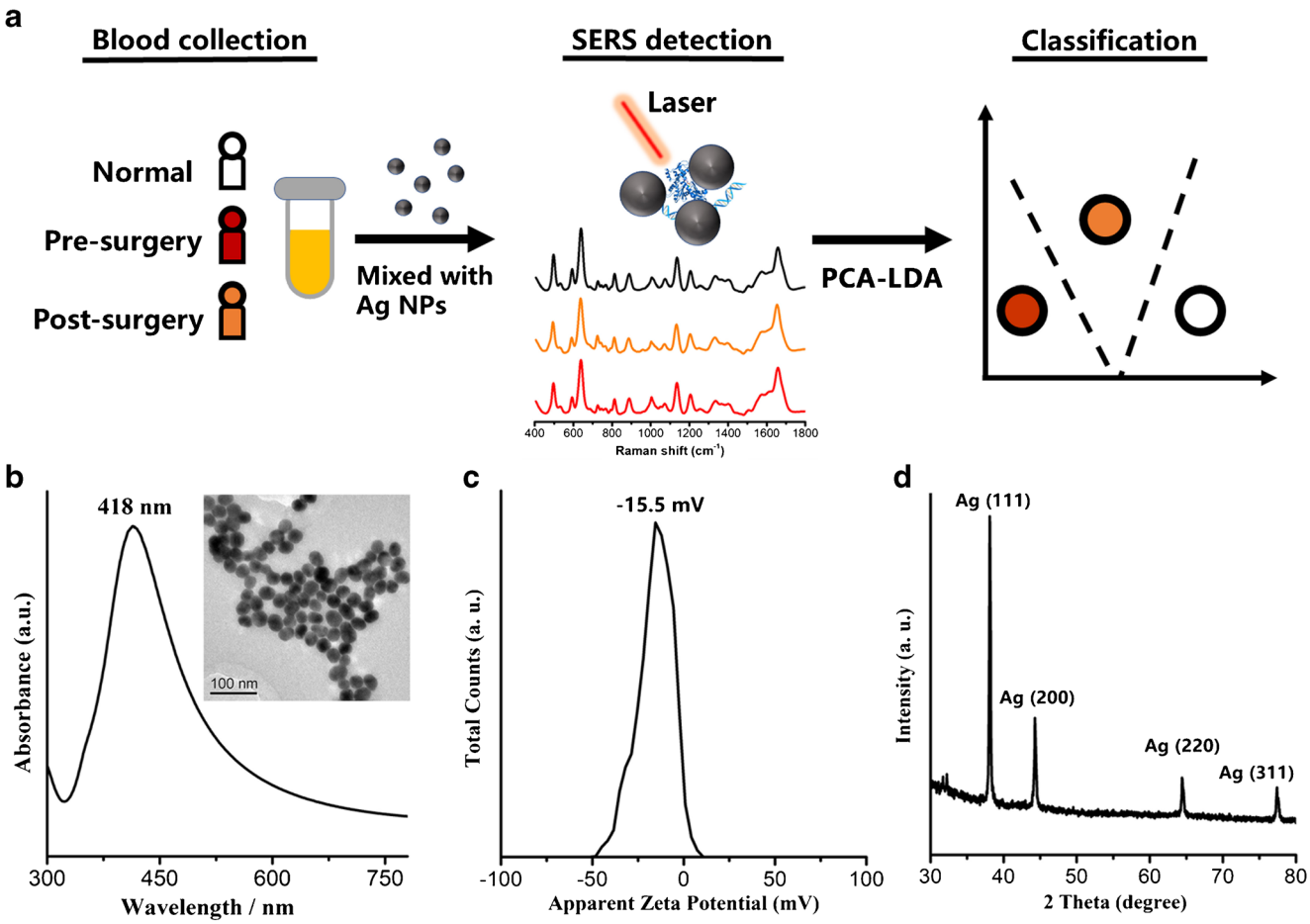

Fig. 1 **a** Scheme of blood SERS detection for classification between pre-surgery vs. post-surgery and pre-surgery vs. normal groups. **b** Absorption spectrum, TEM image. **c** Zeta potential. **d** XRD of prepared Ag NPs

groups. Briefly, PCA was employed to decrease the high dimension of spectral data into a few principle components (PCs) that account for the most of the whole variance in original data while retaining the most diagnostically significant information for sample differentiation. Each loading vector is related to the original spectrum by a variable called the PC score, which represents the weight of that particular component against the basis spectrum, and is capable of reflecting the differences between different groups. Then, the most significant PCs were determined by *T* test using the threshold of 0.05 ($p < 0.05$) and loaded into LDA with the leave-one-out cross-validation method to generate robust diagnostic model to classify different blood groups with sensitivity and specificity results. In this method, one spectrum was removed from the data set and the entire algorithm was redeveloped and optimized using the remaining blood spectra. The optimized algorithm was then used to classify the withheld spectrum. This process was repeated until all withheld spectra were classified [27]. Fig. S2 (see ESM) shows the diagnostically significant PC score plot for the comparison of pre- and post-surgery groups, as well as pre-surgery and normal groups. In this study, PC 1 was identified as the most significant PC for both combinations (pre- and post-surgery groups; pre-surgery and normal groups). Finally, receiver operating characteristic (ROC) curves were plotted based on PCA-LDA data to evaluate the efficiency of blood SERS for breast cancer detection. The SPSS software package (SPSS Inc., Chicago, 18.0) was used for PCA-LDA.

Results and discussion

Using the Ag NPs as SERS substrate, high-quality SERS signal can be fast and easily obtained for each blood sample as shown in Fig. 2. This can be attributed to the electromagnetic enhancement at nanoscale, which dramatically increases the Raman signals of blood components adsorbed onto the surface of Ag NPs. Figure 2 displays prominent Raman peaks located at around 496, 593, 638, 725, 812, 888, 1004, 1072, 1132, 1205, 1331, and 1658 cm^{-1} could be consistently observed in all blood groups, with the strongest signals at 496, 638, 725, 812, 888, 1004, 1132, and 1658 cm^{-1}. Although similar spectral profile, relative intensity changes are detectable for some peaks, such as 496, 638, 725, 1004, 1132, and

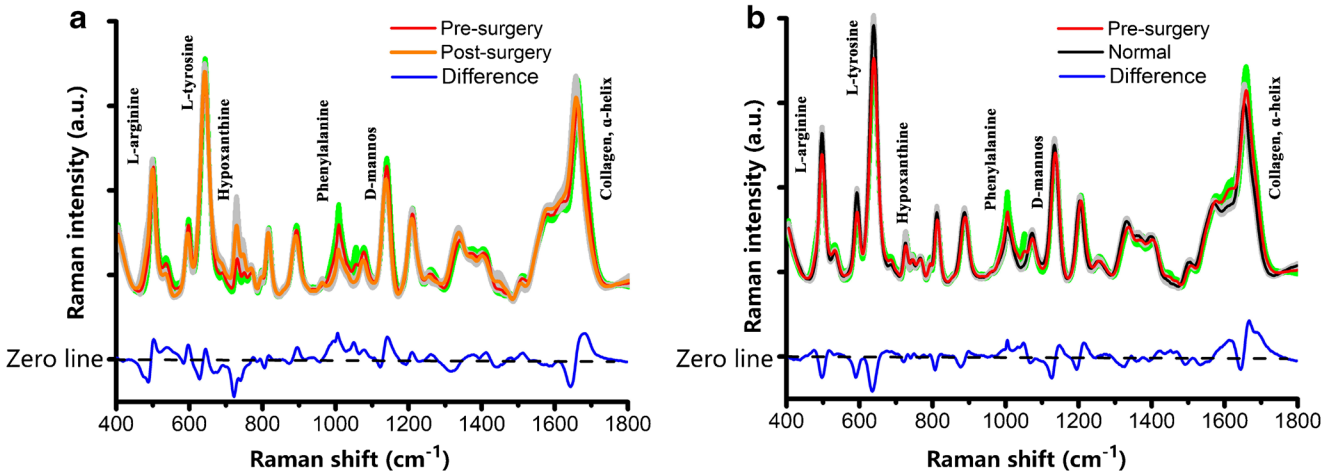

Fig. 2 Comparison of normalized mean SERS spectra from **a** 30 pre-surgery and 30 post-surgery, as well as **b** 30 pre-surgery and 30 normal blood samples. The green and gray shaded areas represent the standard deviations of the means. Also shown at the bottom is the difference spectrum

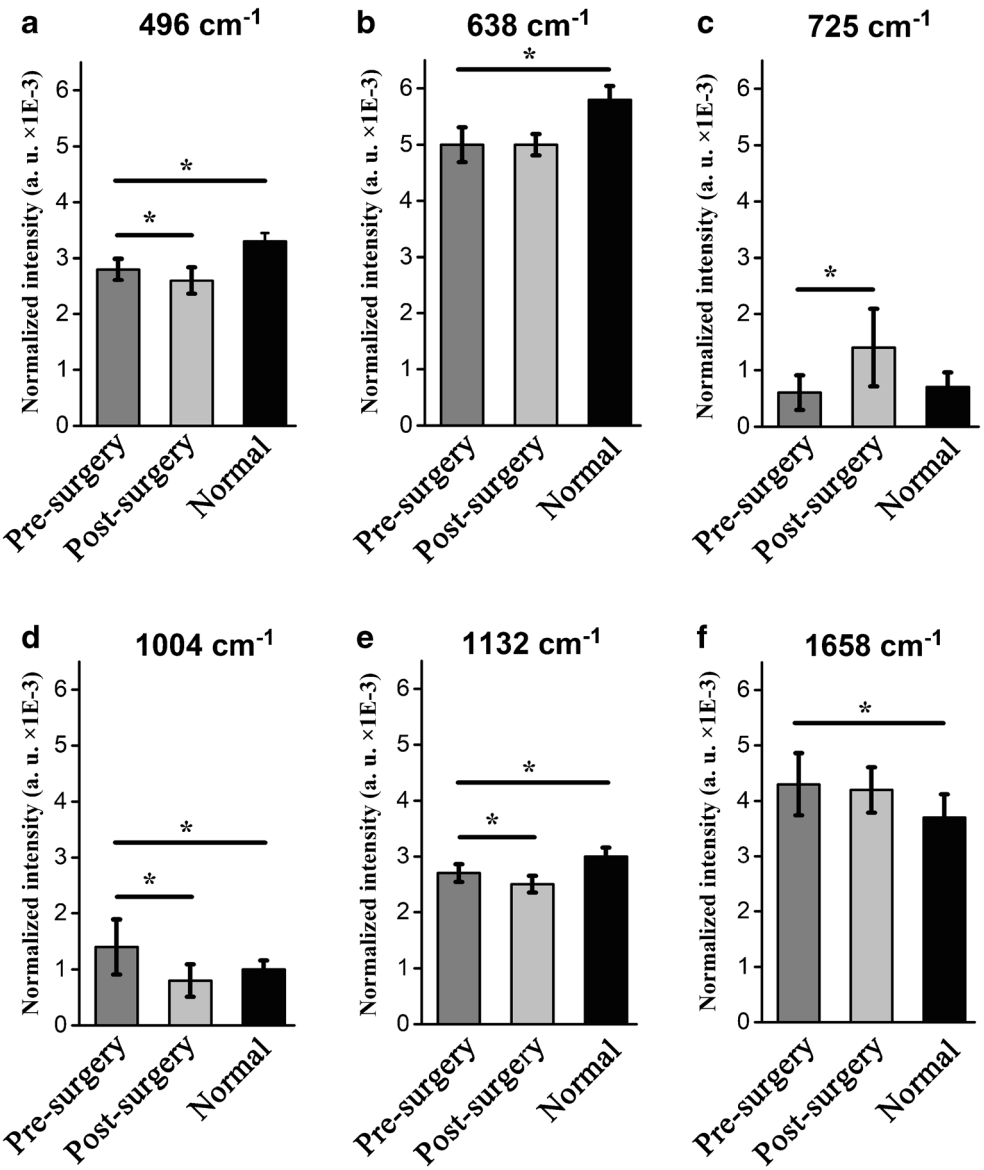

Fig. 3 Histogram of the six peak intensities for the three blood groups: **a** 496 cm^{-1}, **b** 638 cm^{-1}, **c** 725 cm^{-1}, **d** 1004 cm^{-1}, **e** 1132 cm^{-1}, **f** 1658 cm^{-1}. Error bars (whiskers) represent the 1.5-fold interquartile range. *$p < 0.05$ (pairwise comparison with *T* test)

Table 1 The peak positions and tentative assignment of prominent peaks in blood samples [31, 32]

Peak positions (cm^{-1})	Vibrational mode	Major assignment
496	Ring	L-Arginine
593	N/A	Amide VI
638	C–S stretching	L-Tyrosine
725	C–H bending	Hypoxanthine
812	C–C–O stretching	L-Serine
888	C–O–H bending	D-Galactosamine
1004	C–C symmetric stretch	Phenylalanine
1072	C–N stretching	Collagen
1132	C–N stretching	D-Mannose
1205	Ring vibration	Tryphophan
1331	C–H stretching	Nucleic acid bases
1658	C=O stretching	Collagen, α-helix

1658 cm^{-1} after a comparison of mean spactra between pre-surgery and post-surgery, as well as pre-surgery and normal groups (Figs. 2 and 3). In this work, Raman peaks are generated by a variety of substances including proteins, lipid, and nucleic acid (Table 1); meanwhile, corresponding intensities are determined by the concentration of these substances in blood sample. Therefore, analysis of spectral intensities would enable us to explore the distinct changes in blood after surgery operation for breast cancer. As can be seen in Fig. 3, the post-surgery group shows significantly lower intensities at 496, 1004, and 1132 cm^{-1} and higher intensity at 725 cm^{-1}, suggesting a decrease in the percentage of L-arginine, phenylalanine, and D-mannose, and an increase in the percentage of hypoxanthine relative to the total Raman active components in blood sample. On the other hand, significant changes in L-arginine (496 cm^{-1}), tyrosine (638 cm^{-1}), phenylalanine (1004 cm^{-1}), D-mannose (1132 cm^{-1}), and amide I (1658 cm^{-1}) can be found in the pre-surgery (cancer) group in contrast to the normal group. These results are explainable. With tumor development and progression, apoptotic and necrotic cells would release proteins and cell-free nucleic acids due to passive mechanism, or living cancer cells actively release these substances to affect the transformation of susceptible cells at distant sites. When tumor tissues are perfused by blood and lymph, these protein and nucleic acid fragments would enter the circulation, generating unique signatures in circulating blood [28, 29]. When the tumor is removed by surgery operation, the source of these cancer-specific substances is cut off immediately, which eventually makes blood components of post-surgery patients different from those of pre-surgery subjects. Besides, owing to the effect of volatile anesthetics and surgical stress after surgery, immune suppression will appear to effect locoregional and distant metastasis [30]. The specific changes in the relative concentration of molecules associated with these biological processes will be directly represented in SERS spectra, providing a unique way to identify the distinct landscape of blood from post-surgery, pre-surgery, and normal groups.

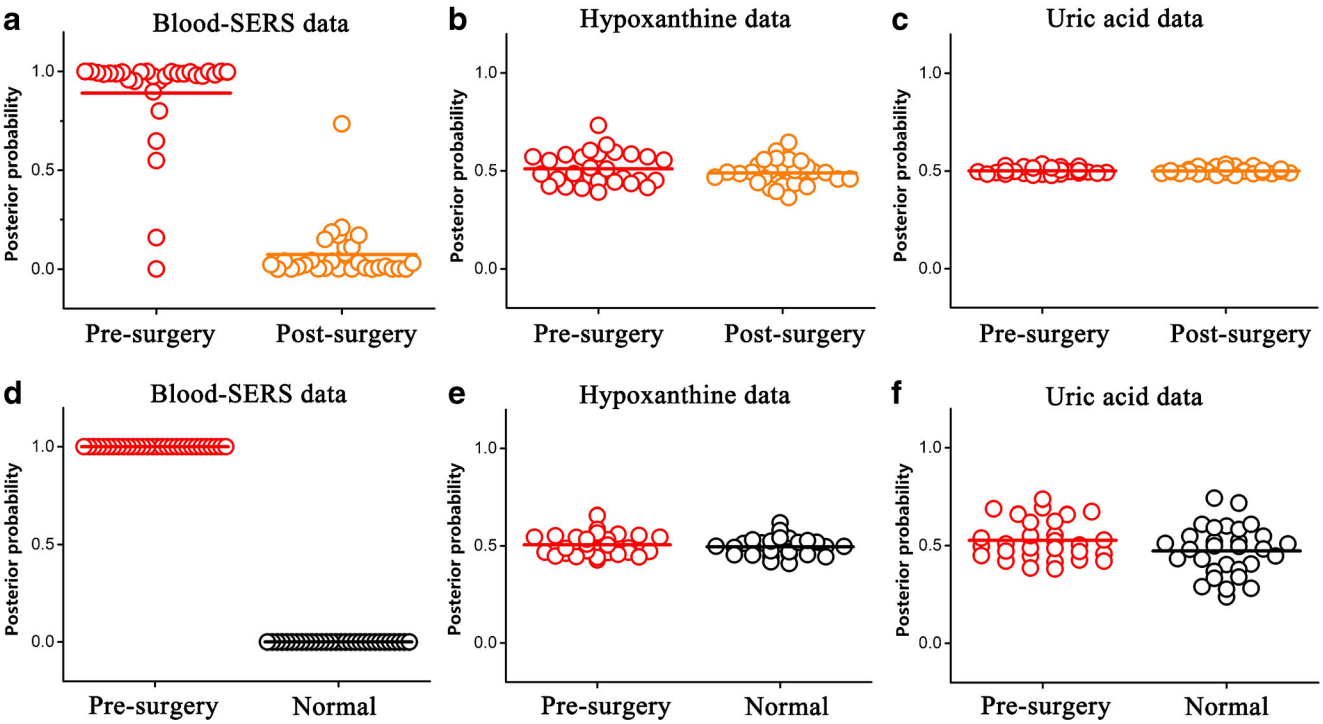

Fig. 4 Scatter plots of the posterior probabilities belonging to **a**–**c** pre-surgery vs. post-surgery groups, and **d**–**f** pre-surgery and normal groups using blood SERS, hypoxanthine, and uric acid data sets

Table 2 Classification results based on blood SERS, clinical hypoxanthine, and uric acid data from the three groups

Diagnostic combinations			Predicted parameters		
			Sensitivity	Specificity	Accuracy
Pre-surgery (blood SERS)	vs.	Post-surgery	93.3% (28/30)	96.7% (29/30)	95% (57/60)
	vs.	Normal	100% (30/30)	100% (30/30)	100% (60/60)
Pre-surgery (hypoxanthine)	vs.	Post-surgery	46.7% (14/30)	63.3% (19/30)	55% (33/60)
	vs.	Normal	46.7% (14/30)	60% (18/30)	53.3% (32/60)
Pre-surgery (uric acid)	vs.	Post-surgery	53.3% (16/30)	43.3% (13/30)	48.3% (29/60)
	vs.	Normal	53.3% (16/30)	56.7% (17/30)	55% (33/60)

Although simple and visualized, above-mentioned intensity analysis still suffers from some disadvantages on lack of ability to analyze the difference of peak shapes, and to identify overlapping peaks. In the context of this, multivariate algorithm based on PCA-LDA was used to automatically explore potential diagnostic information for classifying the three groups. Figure 4a and d show the discriminant models using PCA-LDA for pre-surgery vs. post-surgery and pre-surgery vs. normal groups, respectively. It can be found that the scatter plots representing post-surgery distribute apart from those representing pre-surgery samples with little overlapping, achieving a sensitivity of 93.3% (28/30) and a specificity of 96.7% (29/30). For pre-surgery vs. normal groups, the discriminant efficiency is even better with 100% (30/30) sensitivity and specificity (Table 2). These results suggest that blood samples of patients with breast tumor can be well classified from that of patients without tumor using SERS combined with PCA-LDA algorithm, which may offer a novel and rapid method for preliminarily evaluate the surgical effect. In addition, this technology also may be used for identifying cancer subjects from healthy ones, demonstrating the promising potential for breast cancer screening and diagnosis. The circulating blood contains a variety of biological molecules that are associated with ongoing physiological and pathological events. Thus, blood test is commonly performed to screen or monitor diseases. However, it is impossible to diagnose heterogeneous diseases such as cancer using single marker so far. The alternative way for this goal is to use the entire pattern of blood [29]. Inspired by that strategy, we here used PCA-LDA approach to incorporate the whole SERS spectral information determined by blood components. On the other hand, it should be noted that although some SERS peaks are dominated by uric acid and hypoxanthine [31], other metabolites also make great contributions to the final diagnostic results using this blood SERS method. In order to confirm this, we also analyze the clinic data of hypoxanthine (Fig. 4b, e) and uric acid (Fig. 4c, f) to build the similar diagnostic models for the three groups using LDA algorithm. For hypoxanthine data, only 55% (33/60) and 53.3% (32/60) detection accuracy can be obtained for classifying for pre-surgery vs. post-surgery and pre-surgery vs. normal groups, respectively. Similar poor results with accuracy of 48.3% (29/60) and 55% (33/60) are shown when using uric acid data (Table 2). Moreover, the integration area under the ROC curve (AUC) was used to evaluate and compare the performances using different data sets. For pre-surgery vs. post-surgery

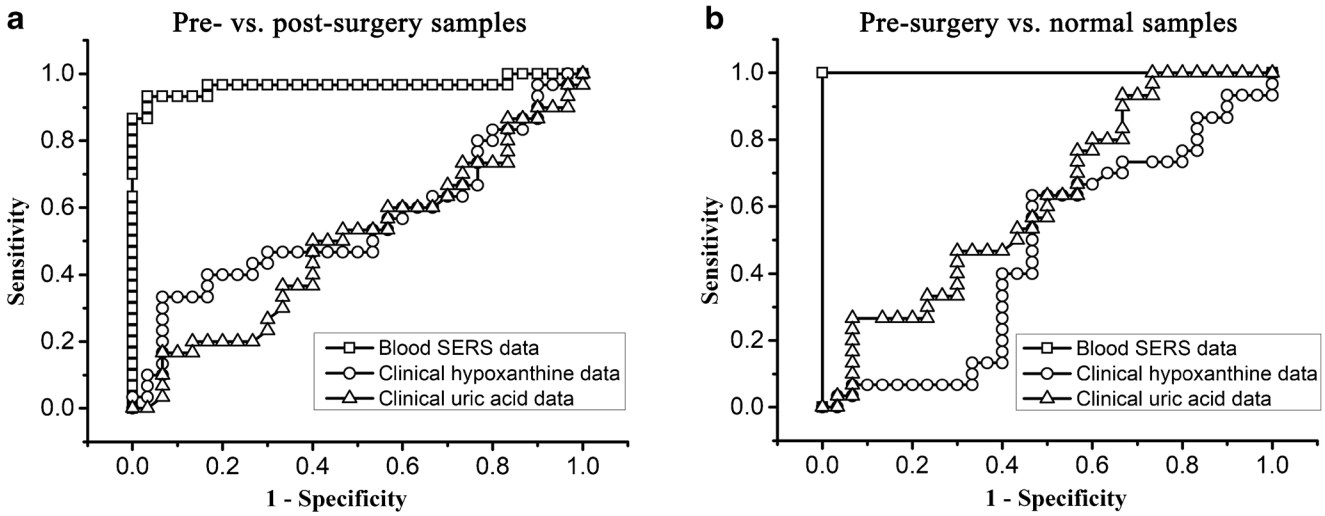

Fig. 5 Receiver operating characteristic curves belonging to **a** pre-surgery vs. post-surgery groups, and **b** pre-surgery and normal groups using blood SERS, hypoxanthine, and uric acid data sets

combination (Fig. 5a), the AUC is 0.964, 0.551, and 0.492 based on blood SERS, hypoxanthine, and uric acid data, respectively. Figure 5b shows the AUC values are 1, 0.539, and 0.617 based on the three data sets for pre-surgery vs. normal combination. It can be concluded that the clinic data of hypoxanthine and uric acid is not diagnostically significant for differentiating the pre-surgery, post-surgery, and normal groups. Besides, the distinct components of blood belonging to specific subjects can be detected by this blood SERS technology, providing a unique blood analysis method for surgery evaluation as well as cancer screening.

Conclusion

In this work, a novel approach for surgical evaluation and screening in breast cancer was developed via blood analysis based on SERS technology combined with PCA-LDA diagnostic algorithm. The subtle changes in the relative concentration of metabolites between post- and pre-surgery, as well as cancer and normal groups, can be detected with the corresponding accuracies of 95% and 100%, respectively. In the next step, much effort should be made to advance this proof-of-concept method. First, more robust SERS substrates need to be designed to improve the sensitivity. Second, large-scale blood analysis is needed to verify the results of this work, and to generate a distinct pattern of blood from subjects with or without tumor. Third, careful follow-up for these patients involved in this study should be performed to explore the possible correlation between cancer outcome and obtained specific spectral pattern. Besides, this technology might be incorporated with portable Raman device to develop a point-of-care detection approach for breast cancer.

Funding information This work was supported by the National Natural Science Foundation of China (Nos. 11974077, 61975031, U1605253, and 61575043); the Innovation Team Development Plan by the Ministry of Education of China (No. IRT15R10), the Natural Science Foundation of Fujian Province of China (No. 2017 J01499) and the Distinguished Young Researcher of Universities of Fujian province of China; and Key Laboratory of OptoElectronic Science and Technology for Medicine of Ministry of Education, China (JYG1908). Science and technology innovation joint fund project (2017Y9089).

Compliance with ethical standards All procedures performed in studies involving human participants were in accordance with the ethical standards of the institutional and/or national research committee (the First Affiliated Hospital of Fujian Medical University, China).

Conflict of interest The authors declare that they have no conflict of interest.

Informed consent Informed consent was obtained from all individual participants included in the study.

References

1. Bray F, Ferlay J, Soerjomataram I, Siegel RL, Torre LA, Jemal A. Global cancer statistics 2018: GLOBOCAN estimates of incidence and mortality worldwide for 36 cancers in 185 countries. CA Cancer J Clin. 2018;68(6):394–424.
2. Lauby-Secretan B, Scoccianti C, Loomis D, Benbrahim-Tallaa L, Bouvard V, Bianchini F, et al. International Agency for Research on Cancer Handbook Working Group. Breast-cancer screening—viewpoint of the IARC Working Group. N Engl J Med. 2015;372(24):2353–8.
3. Pisano ED, Gatsonis C, Hendrick E, Yaffe M, Baum JK, Acharyya S, et al. Digital Mammographic Imaging Screening Trial (DMIST) Investigators Group. Diagnostic performance of digital versus film mammography for breast-cancer screening. N Engl J Med. 2005;353(17):1773–83.
4. Mittal S, Kaur H, Gautam N, Mantha AK. Biosensors for breast cancer diagnosis: a review of bioreceptors, biotransducers and signal amplification strategies. Biosens Bioelectron. 2017;88:217–31.
5. Aravanis AM, Lee M, Klausner RD. Next-generation sequencing of circulating tumor DNA for early cancer detection. Cell. 2017;168(4):571–4.
6. Ma CX, Bose R, Gao F, Freedman RA, Telli ML, Kimmick G, et al. Neratinib efficacy and circulating tumor DNA detection of HER2 mutations in HER2 nonamplified metastatic breast cancer. Clin Cancer Res. 2017;23(19):5687–95.
7. Wang Z, Zong S, Wu L, Zhu D, Cui Y. SERS-activated platforms for immunoassay: probes, encoding methods, and applications. Chem Rev. 2017;117(12):7910–63.
8. Garcia-Rico E, Alvarez-Puebla RA, Guerrini L. Direct surface-enhanced Raman scattering (SERS) spectroscopy of nucleic acids: from fundamental studies to real-life applications. Chem Soc Rev. 2018;47(13):4909–23.
9. Miljanić S, Ratkaj M, Matković M, Piantanida I, Gratteri P, Bazzicalupi C. Assessment of human telomeric G-quadruplex structures using surface-enhanced Raman spectroscopy. Anal Bioanal Chem. 2017;409(9):2285–95.
10. Saranya G, Joseph MM, Karunakaran V, Nair JB, Saritha VN, Veena VS, et al. Enzyme-driven switchable fluorescence-SERS diagnostic nanococktail for the multiplex detection of lung cancer biomarkers. ACS Appl Mater Interfaces. 2018;10(45):38807–18.
11. Shen Y, Yang L, Liang L, Li Z, Zhang J, Shi W, et al. Ex situ and in situ surface-enhanced Raman spectroscopy for macromolecular profiles of cell nucleus. Anal Bioanal Chem. 2019;411(23):6021–9.
12. Lin D, Pan J, Huang H, Chen G, Qiu S, Shi H, et al. Label-free blood plasma test based on surface-enhanced Raman scattering for tumor stages detection in nasopharyngeal cancer. Sci Rep. 2014;4:4751.
13. Stefancu A, Badarinza M, Moisoiu V, Iancu SD, Serban O, Leopold N, et al. SERS-based liquid biopsy of saliva and serum from patients with Sjögren's syndrome. Anal Bioanal Chem. 2019;411(22):1–7.
14. Harmsen S, Huang R, Wall MA, Karabeber H, Samii JM, Spaliviero M, et al. Surface-enhanced resonance Raman scattering nanostars for high-precision cancer imaging. Sci Transl Med. 2015;7(271):271ra7.
15. Sha MY, Xu H, Natan MJ, Cromer R. Surface-enhanced Raman scattering tags for rapid and homogeneous detection of circulating tumor cells in the presence of human whole blood. J Am Chem Soc. 2008;130(51):17214–5.
16. Zheng Z, Wu L, Li L, Zong S, Wang Z, Cui Y. Simultaneous and highly sensitive detection of multiple breast cancer biomarkers in real samples using a SERS microfluidic chip. Talanta. 2018;188:507–15.

17. Cervo S, Mansutti E, Del Mistro G, Spizzo R, Colombatti A, Steffan A, et al. SERS analysis of serum for detection of early and locally advanced breast cancer. Anal Bioanal Chem. 2015;407(24):7503–9.
18. Vargas-Obieta E, Martínez-Espinosa JC, Martínez-Zerega BE, Jave-Suárez LF, Aguilar-Lemarroy A, González-Solís JL. Breast cancer detection based on serum sample surface enhanced Raman spectroscopy. Lasers Med Sci. 2016;31(7):1317–24.
19. Sullivan R, Alatise OI, Anderson BO, Audisio R, Autier P, Aggarwal A, et al. Global cancer surgery: delivering safe, affordable, and timely cancer surgery. Lancet Oncol. 2015;16(11):1193–224.
20. Bleicher RJ, Ruth K, Sigurdson ER, Beck JR, Ross E, Wong Y-N, et al. Time to surgery and breast cancer survival in the United States. JAMA Oncol. 2016;2(3):330–9.
21. Leopold N, Lendl B. A new method for fast preparation of highly surface-enhanced Raman scattering (SERS) active silver colloids at room temperature by reduction of silver nitrate with hydroxylamine hydrochloride. J Phys Chem B. 2003;107(24):5723–7.
22. Rostami-Vartooni A, Nasrollahzadeh M, Alizadeh M. Green synthesis of seashell supported silver nanoparticles using Bunium persicum seeds extract: application of the particles for catalytic reduction of organic dyes. J Colloid Interface Sci. 2016;470:268–75.
23. Ali N, Girnus S, Rösch P, Jr P, Bocklitz T. Sample-size planning for multivariate data: a Raman-spectroscopy-based example. Anal Chem. 2018;90(21):12485–92.
24. Žukovskaja O, Kloß S, Blango MG, Ryabchykov O, Kniemeyer O, Brakhage AA, et al. UV-Raman spectroscopic identification of fungal spores important for respiratory diseases. Anal Chem. 2018;90(15):8912–8.
25. Lin X, Wang L, Lin H, Lin D, Lin J, Liu X, et al. A novel urine analysis technique combining affinity chromatography with Au nanoparticle based surface enhanced Raman spectroscopy for potential applications in non-invasive cancer screening. J Biophotonics. 2019;12(4):e201800327.
26. Lin D, Qiu S, Huang W, Pan J, Xu Z, Chen R, et al. Autofluorescence and white light imaging-guided endoscopic Raman and diffuse reflectance spectroscopy for in vivo nasopharyngeal cancer detection. J Biophotonics. 2018;11(4):e201700251.
27. Huang Z, Lui H, McLean DI, Korbelik M, Zeng H. Raman spectroscopy in combination with background near-infrared autofluorescence enhances the in vivo assessment of malignant tissues. Photochem Photobiol. 2005;81(5):1219–26.
28. Crowley E, Di Nicolantonio F, Loupakis F, Bardelli A. Liquid biopsy: monitoring cancer-genetics in the blood. Nat Rev Clin Oncol. 2013;10(8):472.
29. Liotta LA, Ferrari M, Petricoin E. Clinical proteomics: written in blood. Nature. 2003;425(6961):905.
30. Ramirez MF, Ai D, Bauer M, Vauthey J-N, Gottumukkala V, Kee S, et al. Innate immune function after breast, lung, and colorectal cancer surgery. J Surg Res. 2015;194(1):185–93.
31. Bonifacio A, Dalla Marta S, Spizzo R, Cervo S, Steffan A, Colombatti A, et al. Surface-enhanced Raman spectroscopy of blood plasma and serum using Ag and Au nanoparticles: a systematic study. Anal Bioanal Chem. 2014;406(9–10):2355–65.
32. Feng S, Chen R, Lin J, Pan J, Chen G, Li Y, et al. Nasopharyngeal cancer detection based on blood plasma surface-enhanced Raman spectroscopy and multivariate analysis. Biosens Bioelectron. 2010;25(11):2414–9.